Athermal annealing of pre-existing defects in crystalline silicon

M.D. Mihai[a,e,1], D. Iancu[a,d,1], E. Zarkadoula[b***], R.A. Florin[a,e], Y. Tong[f], Y. Zhang[c,g], W.J. Weber[c**], G. Velişa[a*]

[a]Horia Hulubei National Institute for Physics and Nuclear Engineering, Măgurele, IF 077125, Romania
[b]Center for Nanophase Materials Sciences, Oak Ridge National Laboratory, Oak Ridge, TN 37831, USA
[c]Department of Materials Science & Engineering, University of Tennessee, Knoxville, TN 37996, USA
[d]University of Bucharest, Faculty of Physics, Măgurele, IF 077125, Romania
[e]University Politehnica of Bucharest, RO 060042, Romania
[f]Institute for Advanced Studies in Precision Materials, Yantai University, Yantai, Shandong 264005, China
[g]Energy and Environment Science & Technology, Idaho National Laboratory, Idaho Falls, ID 83415, USA
[1]*Equal contribution*

Abstract

Systematic investigations of electronic energy loss (S_e) effects on pre-existing defects in crystalline silicon (Si) are crucial to provide reliance on the use of ionizing irradiation to anneal pre-existing defects, leading to successful implementation of this technology in the fabrication of Si-based devices. In this regard, the S_e effects on nonequilibrium defect evolution in pre-damaged Si single crystals at 300 K has been investigated using intermediate-energy ions (12 MeV O and Si ions) that interact with the pre-damaged surface layers of Si mainly by ionization, except at the end of their range where the nuclear energy loss (S_n) is no longer negligible. Under these irradiation conditions, experimental results and molecular dynamics simulations have revealed that pre-existing disorder in Si can be almost fully annealed by subsequent irradiation with intermediate-energy incident ions with S_e values as low as 1.5 - 3.0 keV/nm. Selective annealing of pre-existing defect levels in Si at room temperature can be considered as an effective strategy to mediate the transient enhanced diffusion of dopants in Si. This approach is more desirable than the regular thermal annealing, which is not compatible with the processing requirements that fall below the typical thermal budget.

* Corresponding author. Horia Hulubei National Institute for Physics and Nuclear Engineering, Măgurele, IF 077125, Romania
E-mail addresses: gihan.velisa@nipne.ro (Gihan Velişa), Tel: +4 0723-933-922

** Corresponding author. Materials Science and Engineering, University of Tennessee, Knoxville, TN 37006, USA.
E-mail addresses: wjweber@utk.edu (William J. Weber), Tel: +1 865-974-0415

*** Corresponding author. Center for Nanophase Materials Sciences, Oak Ridge National Laboratory, Oak Ridge, TN 37831, USA.
E-mail addresses: zarkadoulae@ornl.gov (Eva Zarkadoula)

1. Introduction

Ion-implantation doping process has emerged as an essential device manufacturing technique in the semiconductor industry, and especially in the fabrication of silicon-based devices (e.g., silicon-based microelectronics [1,2] and silicon-based quantum computing [3]). Its main drawback is that the ion implantation doping process goes hand-in-hand with implantation-induced defects, and recovery of the original crystalline structure of Si is crucial to maximize the density of electrically active dopants sites [4,5]. The removal of defects is also pivotal for suppression of unwanted electrically active defect structures [5]. A commonly employed method to anneal defects is thermal annealing, and unfortunately, this is what usually enables the transient enhanced diffusion in Si [6,7]. In this case, the influence of this diffusion process on the activation of dopants are assumed to have deleterious effects [8]. As a result, several studies have focused on understanding of either low-energy ion [4,9] or high-energy ion [10,11] irradiations effects on crystalline Si, because in general, the irradiation-induced damage evolution in semiconductors and insulators can be rationalized using the energy loss (or energy) of ions as key parameter, and Si does not make an exception to this rule. In its simplest description, the energy loss of ions can be partitioned between energy transferred to target atoms via elastic interactions with the target atoms, well-known as nuclear energy loss (S_n), and the energy transferred to electrons via inelastic interactions, well-known as electronic energy loss (S_e) [12,13]. It is well established that S_n is dominant at low energies ($E \leq 1$ keV/amu), while S_e is dominant for high-energy ions, especially for swift heavy ions (SHIs), ($E > 1$ MeV/amu) [12]. For example, researchers have reported that low-energy ion irradiation leads to amorphization of Si, if the irradiation temperature does exceed the critical amorphization temperature, T_C (~400 K) [14]. Here, it is worth making a comment that if the irradiation is performed above T_C, the formation of amorphous Si is hindered due to dynamic annealing [15]. The origin and sources of dynamic annealing were rather recently investigated and well documented in seminal papers [16–18], as well as S_n-induced damage accumulation and amorphization processes, have been previously reviewed [4,9,15]. Briefly, in these reviews, the researchers have concluded that Si is very sensitive to S_n-induced damage accumulation, since Si is easily amorphized under low-energy ion irradiation performed at room temperature.

On the other hand, experimental studies on the response of undamaged Si to high-energy ion irradiation (S_e-regime) have shown that highly ionizing irradiation (e.g., 3.6 GeV U ions, $S_e \sim 28$ keV/nm [11]) will only produce weak damage, i.e., point defects and point defect complexes [10]. The exception is for cluster ions (e.g., 30 MeV C_{60}, $S_e \sim 46$ keV/nm [19]),

where clear evidence for the generation of ion tracks was found in early studies [19,20], due to higher S_e values compared to monoatomic ions [12]. More recently, the formation of ion tracks in Si has also been observed at much lower intermediate cluster energies (e.g., 1-6 MeV C_{60}, S_e = 8.5-18.2 keV/nm) [21] than previously reported. This finding was tentatively ascribed to the synergistic effects between S_n and S_e, since in the intermediate energy regime both S_n and S_e are significant to promote either the synergistic or competitive effect [13,22], without excluding that the transient boiling-melting transitions with recrystallization processes may also be the reason behind ion track formation. If the synergistic effect is active, it may trigger the formation of ion tracks [13]. In the same study, the authors have revealed that no ion track formation is observed under 200 MeV Xe ions irradiation (S_e = 14 keV/nm) [21]. This same study, among other studies, has also highlighted the importance of understanding and predicting defect production and evolution in the intermediate-energy regime (i.e., up to ~50 keV/amu), where ionization (driven by S_e) processes is occurring simultaneously with ballistic cascade processes (driven by S_n). One should note that separating and quantifying the contributions of S_e and S_n to defect production and evolution, when both processes are occurring simultaneously, is not straightforward. Apart from simultaneous dual beam experiments involving low- and high-energy incident ions to trigger to S_n- and S_e-driven processes [14,23–25], respectively, sequential dual beam experiments can also be used to enrich the understanding of coupled defect evolution and recovery [13,22]. In these sequential dual beam experiments, pre-existing defects or an amorphous layer is initially created in the near-surface (< 1000 nm) of crystalline Si via low-energy ion irradiation through S_n-driven processes [26]. Then the separate response of the pre-existing damage to S_e is evaluated by a successive irradiation with high-energy ions (S_n is negligible over this near-surface region). For reference, undamaged Si should be irradiated under same experimental conditions with high-energy ions. Note that simultaneous and sequential dual beam experiments are usually labeled as S_n & S_e and S_n + S_e, respectively.

As a result, several studies [15,27–30] have focused on understanding the effects of high-energy ions subsequently impinged onto a pre-damaged Si by using low-energy ions irradiation, which is pivotal for semiconductor industry. Of course, many of these studies have also triggered by a considerable scientific interest in understanding the fundamentals of the coupled effects of S_e and S_n on nonequilibrium defect evolution in Si [12], which remains a very attracting research topic up today [24,31]. These studies have reported that recrystallization of an amorphous Si layer can be accomplished when exposed to successive irradiation with ions that deposit their energy inside the amorphous layer. The recrystallization process was achieved under room-temperature SHI irradiations, the so-called SHI-induced ion

beam-induced epitaxial crystallization (SHIBIEC) process [5,31]. Interestingly, the recrystallization process was also achieved under low-energy ion irradiations, but at irradiation temperatures higher than room-temperature (≥ 473 K) [29], the so-called ion beam induced epitaxial crystallization (IBIEC) process [29,32]. Surprisingly, such an annealing process was also reported to occur even under light-ion irradiation, such as 200 keV H and He, performed at room-temperature [33,34]. It is well established that the SHIBIEC process is triggered by the S_e-induced annealing (excitation and ionization) or athermal processes [13], while the IBIEC process occurs as a consequence of S_n-induced migration and recombination of defects at the amorphous/crystalline interface [35]. More recent studies [14,24] have demonstrated that simultaneous dual beam experiments, using low-energy 900 keV I ions and high-energy 27 MeV Fe (S_e = 5.5 keV/nm) or 36 MeV W (S_e = 5.5 keV/nm) ions, can also lead to efficient ionization-induced annealing in Si. This process is known as synergy between nuclear and electronic energy losses [23]. The SHIBIEC process observed under SHI irradiations has also been observed at much lower intermediate energies (such as 10 MeV Co, S_e = 4.0 keV/nm) in pre-damaged Si [26]. Ion-beam-induced annealing of pre-existing point defects in Si at 300 K has been also observed by Holland[36] under 1.25 MeV Si ions irradiations, which is providing the interstitial population needed to anneal the divacancy constituent of the pre-existing damage. Annealing of pre-existing defects in Si occurs even during neutron irradiations at temperatures below 370 K [37].

In contrast to high-energy irradiation studies, there have been only a few studies devoted to intermediate-energy irradiation regime [14,24,26] that could facilitate the successful implementation of ionization-induced annealing technology in the fabrication of silicon-based devices. Thus, the response of pre-damaged Si to ionizing irradiation not only using ions with high S_e value but also ions with much lower S_e values than previously reported (4 keV/nm) [26] should be investigated. Of course, these studies should also be driven by a considerable scientific interest in understanding the fundamentals of coupled effects of S_e and S_n on nonequilibrium defect evolution in Si. In this regard, the present study addresses the separate effects of different S_e values on nonequilibrium defect evolution in pre-damaged Si at 300 K using O and Si ions both at 12 MeV, and the results reveal that pre-existing disorder in Si (~70%) can be almost fully annealed by ions with S_e values as low as 1.5 - 3.0 keV/nm. It should be noted that the S_e values used in the present study are well below those previously reported in sequential dual ion beam approach (4 keV/nm) [26].

2. Experimental and modeling details

2.1. Irradiation and characterization

In this study, four monocrystalline silicon samples used for irradiation were cut from an undoped <100>-oriented Si wafer (https://www.alineason.com/) with a single-side epi-polished surface. The samples were approximately 10 × 10 mm^2 in size, with thickness of 0.5 mm. In the first step of the experimental procedure, a pre-damaged state with a shallow range distribution (< 1200 nm) was initially introduced in one set of two Si samples via ion irradiation with 2.0 MeV Au ions to an ion fluence of 0.3 ions nm^{-2}. In the second step of the experimental procedure, the separate response of the pre-damage state to S_e was evaluated by a successive irradiation with intermediate-energy ions (12 MeV O and 12 MeV Si ions) that interact with the pre-damaged surface layers of Si mainly by ionization, except at the end of their range, beyond the pre-damaged layers, where the S_n is no longer negligible. In the latter step, for reference, an additional set of two virgin (undamaged) Si samples were also irradiated with 12 MeV O and 12 MeV Si ions under identical conditions. All ion irradiations were carried out at 300 K and off-channel direction (7° off main channeling direction) to minimize ion channeling effects. The average ion flux during ion irradiation experiments was kept below 5 × 10^{10} $cm^{-2}s^{-1}$, for the indicated ion species. In between each irradiation step, *ex-situ* Rutherford backscattering spectrometry in channeling geometry (RBS/C) was conducted, using 2 MeV He particles, to quantify the evolution of the pre-damage state following irradiation with intermediate energy ions having S_e value intervals way below that previously reported in sequential dual ion beam approach. In order to detect the backscattered He particles, a silicon detector was positioned at 155° with respect to the He analyzing beam direction. All these ion species (He, O, Si and Au) were delivered by the 3 MV Tandetron Cockcroft-Walton accelerator located at IFIN-HH, Magurele, Romania [38,39]. The S_n and S_e values were calculated using the Stopping and Range of Ions in Matter (SRIM-2003) code [40] in a full cascade mode [41] with input density given by the manufacturing company (2.329 g cm^{-3}). The corresponding local damage dose in displacements per atom (dpa) were also calculated, for the indicated ion fluences in Table 1, via SRIM-2003 with a threshold displacement energy of 20 eV [42] used as input. The output of the SRIM calculations is reported in Table 1.

Table 1: SRIM-depicted S_n, S_e, and ratio S_e/S_n at the Au-induced damage peak (~540 nm) in Si for indicated ion species. The dpa for the indicated ion fluences is also included.

Ion/energy	S_n (keV/nm)	S_e (keV/nm)	S_e/S_n	dpa @ ~532 nm
2 MeV Au	2.48	1.88	0.75	0.20 (0.3 Au^+ nm^{-2})
12 MeV O	0.002	1.58	790	0.02 (40.0 O^+ nm^{-2})
12 MeV Si	0.014	3.05	217	0.04 (20.0 Si^+ nm^{-2})

Transmission electron microscopy (TEM) thin foils were prepared by a gallium focuses ion beam lift-out technique (Amber, Tescan). TEM operated at 200 kV (Talos F200X G2) was utilized to study the atomic structure of irradiated samples.

2.2. Modeling details

For the molecular dynamics (MD) simulations, we used the DL_POLY MD code [43] and a modified Tersoff potential for Si by Kumagai et al [44]. The systems used have size 10 nm × 10 nm × 5 nm size, which is large enough for studying the effects of energy deposition and dissipation from 12 MeV O and Si ions. The pre-damage levels were introduced by creating different percentages of Frenkel pairs (FPs), and then equilibrating the systems under constant pressure and temperature at 300 K with 1 fs timestep for about 0.5 to 1.5 ns. The defects were identified using the sphere criterion, with a cut-off radius of 0.75 Å [43,45,46]. The irradiation simulations were performed by employing the two-temperature model (2T-MD), suitable to simulate irradiation simulations in metals [47–49] and semiconductors or insulators [50,51], where the energy deposition to the electronic subsystem from the fast-moving projectile is transferred to the atomic subsystem via electron-phonon coupling. We used systems with four pre-damage levels, 5.5% FPs, 7.2% FPs, 10.2% FPs and 14.4% FPs, where this pre-damage level represents the percentage of stable FPs after the equilibration of each system. In each system, 200 ion irradiations were performed, where the irradiation was applied along the z dimension of the MD box where the ion path is at the center of the xy plane, in intervals of 5 ps, which was long enough for the energy to dissipate and the system to cool down. The electronic diffusivity temperature dependence is described by $D_e(T) = D_0 \frac{T_0}{\min(T,T_f)}$ as described in [43], where D_0 is the value at room temperature (33.6 cm2 s−1 [52]), and T_f is the Fermi Temperature. The electronic heat capacity dependence on temperature is described in [53]. As in [51], the electron-phonon relaxation time was taken to be 0.26 ps.

3. Experimental and Modeling results

The RBS spectra recorded along the <100> axis for Si single crystal irradiation with 2.0 MeV Au ions to an ion fluence of 0.3 ions nm^{-2}, together with the RBS spectra recorded along the main axis and "off"-axis (random direction) for unirradiated sample, are illustrated in Fig. 1(a). Note that from the RBS/C viewpoint, irradiated Si is considered to be rendered amorphous when the aligned RBS yield is similar in magnitude with the corresponding random RBS yield [15]. Therefore, the lower the aligned RBS yield the better is the crystalline quality of Si. The RBS/C spectrum from the unirradiated Si (orange filled diamonds) is characterized by a small axial minimum yield ($\chi_{min} \sim 0.025$ at about channel 350), which demonstrates that high-quality single crystals have been used in this study. Irradiation with Au ions leads to the development of well-resolved damage peak in the RBS/C spectra (black open circles), which provides clear evidence that the observed atomic disorder in Si consists of uncorrelated displaced lattice atoms, such as point defects, clusters of point defects and amorphous regions [54]. Although Au irradiation induces a significant increase in ion channeling yield, it is still situated way below the random (amorphous) level. Subsequent irradiation with 12 MeV O ions to an ion fluence of 8.0 ions nm^{-2} produces a decrease in ion channeling yield (green filled triangles) over the entire damage profile. It should be noted that the aligned RBS yield keeps decreasing with increasing O ion fluence, indicating the occurrence of an annealing process. A similar trend is observed for the pre-damaged sample and subsequently irradiated with 12 MeV Si ions case (see Fig. 1(b)). In the high channel region (220-350), ion channeling analyses of 12 MeV O irradiated pristine Si shows a small increase in the backscattering yield compared with RBS/C spectra recorded for unirradiated sample, indicating that a very small number of defects is produced via 12 MeV O ion irradiation. On the other hand, in the low channel region (i.e., deeper depth), a slight increase of dechanneling component with O fluence is observed, as compared to the pristine sample. This effect is likely generated by the S_n part of the slowing-down of 12 MeV O ions since at the end of their range, S_n no longer has a negligible impact. Although quantifying the disorder in the end of ion path is not within the focus of this study, as a first estimation, the difference in minimum yield of irradiated and pristine (unirradiated) crystalline sample, $\Delta\chi_{min} = \chi^{irr}_{min} - \chi^{prist}_{min}$, can be used to quantify the O-irradiation induced damage in pristine Si at different channels or depths. The calculated values of $\Delta\chi_{min}$ for channel number 288 (at the Au-induced damage peak) and 150 (i.e., deeper depth), respectively, are plotted in the inset of Fig. 1 (c) for O-irradiated Si to ion fluence of 40.0 ions nm^{-2}, respectively. This inset confirms that pristine Si starts to be relatively more damaged under O ions

irradiations once we move to greater depths. In other words, highly damaged or amorphous buried layer is expected to be created at the end of ion range. The ion channeling data recorded on pristine Si irradiated with 12 MeV Si (see Fig. 1(d)) follow nearly the same trend as the 12 MeV O irradiation of pristine Si (i.e., a slight increase of dechanneling component with Si fluence is observed, as compared to the pristine sample); however, one should note that the fluence needed for the aligned spectrum (dechanneling component in the low channel region) to reach almost the same yield is a factor of two lower for Si ions (20.0 ions nm^{-2}) than for O ions (40.0 ions nm^{-2}). This indicates that 12 MeV Si irradiation disorder accumulation displays a more rapid initial rate of disordering, as compared to 12 MeV O irradiation. According to SRIM predications (see Table 1) for 12 MeV Si, S_n is the highest among the two different ion species used in the current study, and thus it is expected that this effect is likely generated by the S_n part of the slowing-down of 12 MeV S ions. On the other hand, our ion channeling results reveal no significant differences, beyond experimental uncertainty, in the aligned RBS yield of the Si-irradiated pristine Si to ion fluence of 10 and 20.0 ions nm^{-2}. This indicates that the damage accumulation saturates due to a competition between damage production from S_n and athermal annealing associated with S_e, as seen previously for 15 MeV Si irradiation of SiC [55], despite the fact that data at higher irradiation fluences are absent. It should also be mentioned that the saturation in dechanneling component (disorder) for the 12 MeV Si ion is consistent over multiple channels (depths). All these effects suggest that S_n-induced defect generation is initially dominant at low fluences, while the contribution of the S_e-induced athermal annealing dominates at higher fluences (see MD results).

Fig. 2(a) illustrates the corresponding depth profile of relative Si disorder for the pre-damaged Si prior to and after following 12 MeV O ions irradiations obtained by analyzing RBS/C spectra (see Fig. 1(a)) employing an iterative procedure (IP) described in detail elsewhere. Briefly, under the IP, the measured relative disorder equal to 1.0 stands for random (amorphous) state; whereas zero stands for pristine (undamaged) state. Note that Fig. 2 (b) provides the evolution of pre-existing damage peak after sequential 12 MeV Si ion irradiations. The smooth line fits to data points are superimposed for visual clarity. Also superimposed are S_e curves across the pre-existing damage peak (see dash-dot lines). In this depth region (i.e., $0 < z < 1200$ nm), S_e values are nearly constant and by a factor of approximately 780 and 200 higher than the S_n values for O and Si ions (see Table 1), respectively. As shown in Fig. 2, Au ion irradiations to ion fluences of 0.3 ions nm^{-2} (see black open circles) has induced an initial maximum level of fractional disorder (f_0) of ~ 0.7 on the Si lattice. According to previous amorphization kinetics that proceeds in three steps [15], the sample with $f_0 \sim 0.7$, corresponds

to the second part of step 2, and thus the damage morphology is likely governed by mixture of damaged crystalline and amorphous Si phases (the latter one starting to become dominant) [15]. Sequential irradiations with either O or Si ions lead to a systematic decrease of the relative disorder magnitude with increasing ion fluences. Note, however, that the value of ion fluence at which almost complete healing of defects ($f_0 \leq 0.2$) is substantially dependent on the ion species (~ 40.0 ions nm^{-2} for O and ~20.0 ions nm^{-2} for Si). The difference in annealing fluence may result from the higher S_e value of Si ions than the O ones in this depth region, which could directly influence the annealing kinetics (see discussion below).

Fig. 3 (a) presents a HRTEM micrograph recorded at Au-induced damage peak (~532 nm) on a Si single crystal irradiated with 2.0 MeV Au ions to an ion fluence of 0.3 ions nm^{-2} at 300 K. The micrograph indicates that most of the defects created during Au irradiation at the indicated ion fluence are amorphous pockets surrounded by distorted crystalline regions. Moreover, the mixture of highly disordered and amorphous phases at this depth is confirmed by the fast Fourier transform (FFT) analyses, shown in the inset of the figure, which exhibits structure spots and diffuse scattering. In the case of pre-damaged Si sample and subsequently irradiated with 12 MeV O ions to an ion fluence of 40.0 ions nm^{-2} at 300 K, the HRTEM micrograph recorded at the same depth of Au-induced damage peak (see Fig. 3 (b)), shows that 12 MeV O ions can heal the pre-existing defects, as revealed by RBS/C (Fig. 1(a)). The recrystallized character (less damaged) of the sample at this depth is confirmed by the FFT analysis shown in the inset of the figure (less visible diffuse scattering rings). The HRTEM micrographs of Fig. 3 (a) and (b) were further processed using inverse FFT filtering in order to improve the visibility of microstructure modification of pre-damaged Si upon subsequent O irradiation, and the results are shown in Fig. 3 (c) and (b), respectively. The annealing of amorphous pockets surrounded by distorted crystalline regions (main component of the pre-damaged layer) under 12 MeV O ions irradiations indicates the occurrence of epitaxial recrystallization, which may be identified as the main mechanism responsible for the ion-beam-induced annealing observed the current study.

Fig. 4 displays the level of damage in four systems with pre-existing defects for 12 MeV Si (a) and 12 MeV O (b) irradiation, as a function of the number of ions. For comparison, damage evolution in the pristine sample for increasing number of Si ions is also provided (Fig. 4(c)). It is observed that at early stages of the irradiation, more damaged is induced due to 12 MeV Si ions compared to 12 MeV O ions. It is additionally seen that annealing of Si is easier under the 12 MeV Si ions irradiation at later stages, compared to 12 MeV O ions, with annealing ranging from ~40% to ~52% for Si ions and ~3% to ~20% for O ions. These results also show

that with increasing pre-existing damage level recovery of more defects takes place. The MD results for Si irradiation of undamaged material reveals that damage is initially created within the effective volume of the thermal spikes, which are recrystallized for increasing number of ions, with a few points defects surviving (see Supplementary Movies to visualize the entire athermal recrystallization process). This finding is in good agreement with our ion channeling spectra recorded on Si-irradiated undamaged material (see Fig. 1(d)), that indicates S_n-induced defect generation is initially dominant at low fluences, while the contribution of the S_e-induced athermal annealing is counterbalanced at higher fluences. For irradiation with 100 O ions of 12 MeV energy, there is no damage production except for a couple of FPs that are annealed, which is also in good agreement with ion channeling spectra (see Fig. 1(c)) recorded on O-irradiated pristine Si that illustrated no noticeable damage was created at channel number 288 (at the Au-induced damage peak).

4. Discussion

Athermal transient phenomena are typically characterized by their weak or temperature-independent nature, making them distinct from thermally activated processes [13]. These transient processes often precede radiation-enhanced effects that occur over longer time scales, especially in relation to the high concentration of nonequilibrium defects. As described above, we can almost fully heal the pre-existing disorder levels in Si (from 0.7 to below 0.2) via subsequent irradiation at room temperature with either 12 MeV O or 12 MeV Si ions, although the value for the ion fluence where disorder level is below 0.2, determined using RBS/C, is ion species-dependent due to the different amounts of S_e deposited in the pre-damaged layer. As stated in the Introduction, the recovery of pre-damaged state in Si has also been observed under 10 MeV Co ions (S_e = 4.0 keV/nm) irradiation at 300 K [26], similar to the case of O and Si ions in the present study. In this same experimental study, the authors have associated the observed damage reduction with ionization-induced damage annealing process. In other independent ion irradiation studies of Si, such as simultaneous dual beam experiments, using low-energy 900 keV I ions and high-energy 27 MeV Fe (S_e = 5.5 keV/nm) or 36 MeV W (S_e = 5.5 keV/nm) ions [14], it has also been observed that the damage level decreases with rising fluence of ionizing ions, an effect that was also associated with ionization-induced damage annealing process.

Previously it was also shown that the annealing of amorphous [36,56] or weakly damaged [36] Si can be achieved via subsequent irradiation with either 3 MeV Ne (S_e ~1.7 keV/nm) ions [56] or 1.25 MeV Si (S_e ~1.2 keV/nm) ions [36], respectively. These same studies

have revealed that such ion beam annealing (IBIEC process) is a defect-mediated process. At these energy ranges, S_n is no longer negligible, such as in the present study, and thus the IBIEC process occurs as a consequence of irradiation-induced defects that are able to migrate and thus, to recombine at the amorphous/crystalline interface [35]. This is also supported by the work of Kinomura et al [37] who reported recovery of pre-damaged Si under neutron irradiation at an estimated temperature of maximum 370 K. In the present study, the S_n and dpa values at the Au-induced damage peak (see Table 1), for both ion species, are too weak to inflict the damage necessary (see Fig. 1(c)) to mediate the activation of IBIEC process. In other words, these observations unambiguously demonstrate that the annealing process observed in the present study is a consequence of local electronic excitation processes.

In order to compare the susceptibility of pre-damaged Si to ionization-induced recovery and consequently to assess the recovery cross-sections (σ_r), the normalized recovery of relative Si disorder at the damage peak (N/N_0) as a function of both O and Si fluences are depicted in Fig. 4. These plots clearly follow the same exponential decrease with rising fluence (Φ) of intermediate-energy ions, as reported previously in other pre-damaged crystalline materials, such as SiC [57], $SrTiO_3$ [58] and $KTaO_3$ [22]. The following formula has been used to model this dependence:

$$N/N_0 = 1 - N_r/N_0 \times [1 - \exp(-\sigma_r \times \Phi)], \quad (1)$$

where N_r/N_0 denotes the recoverable fraction of disorder at the damage peak. Fits of [Eq. (1)] to the experimental data are shown in Fig. 5 as solid lines, and the derived fitting parameter (σ_r) for O and Si ions are depicted in Fig. 5. This is expected to be consistent with the previous, theoretical calculations performed for other semiconductors or insulators, which have revealed that with increasing S_e value much higher temperatures during the transient thermal spike are obtained, leading to increased susceptibility of pre-damaged material to damage annealing[57]. Since the S_e value for 12 MeV Si ions is higher than that of 12 MeV O ions, this interpretation could also be envisioned for the present results.

For a more comprehensive picture on the physical processes behind the irradiation-induced annealing process revealed by RBS/C measurements and TEM observations, as presented above, the evolution of pre-existing defects in Si under ionizing ions was simulated using MD simulations. It was observed that the energy depositions from 12 MeV Si and 12 MeV O ions can result in the formation of some additional damage during the interactions with

ions, but the local heating (i.e., thermal spike) and defect diffusion processes result in the recombination of defects and epitaxial recrystallization. The higher local temperature due to the larger energy deposition from 12 MeV Si ions, compared to that from 12 MeV O ions, enhances the recombination of defects compared to the level of annealing observed in 12 MeV O irradiation of Si, which is consistent with the RBS/C results.

Finally, it is to be noted that the thermal spike due to the ion irradiation has been modelled with the ion path along the z axis and passing from the center of the xy plane. While the defects in the volume of the whole MD box are counted to capture recombination because of diffusion due to the thermal spike-induced temperature, there is an effective cylinder along the ion path where most of the damage formation and recombination take place. The recombination in the effective region is reflected in the more rapid drop compared to experiment of defect concentration in the Fig. 4 (a). Experimentally, the area that is measured is larger and contains the effect of more ions/thermal spikes, including their effective volumes and areas in-between. Both in MD and experiment, the ability of the system to recover under 12 MeV Si and O ions is demonstrated and is in good agreement.

5. Summary

To summarize, we have successfully demonstrated that pre-existing disorder in Si can be almost fully recovered (from 0.7 to below 0.2) by subsequent irradiation with either 12 MeV O or 12 MeV Si ions due to the inelastic thermal spike that can sufficiently raise the local temperature along the ion path and provoke defect recovery and epitaxial recrystallization of amorphous domains (so called ionization-induced recovery process). Compared to previous ionization-induced recovery reported for pre-damaged Si, the current study demonstrates that the same process is driven by ions with much lower S_e values than reported to date, gaining crucial data that can contribute greatly to model the crystallization process at this intermediate-energy regime. For O and Si ions, the recovery cross-sections increase from 0.039 to 0.168 nm^2 with increasing S_e values from 1.58 to 3.05 keV/nm. The molecular dynamics simulations results have further fortified the substantial role of local electronic excitation processes in annealing process observed in the present study. While such ionization-induced annealing or athermal process may offer a useful alternative to overcome the thermal budget associated with regular thermal annealing and dopant activation, the understanding of such phenomenon can contribute significantly to our basic understanding of competitive effects in Si.

Acknowledgments

This work was supported under Research Programme Partnership in Priority Areas PNII MEN-UEFISCDI, contract PN 23210201. Experiments were carried out at 3 MV Tandetron™ accelerator from “Horia Hulubei” National Institute for Physics and Nuclear Engineering (IFIN-HH) and were supported by the Romanian Government Programme through the National Programme for Infrastructure of National Interest (IOSIN). This research used resources of the Compute and Data Environment for Science (CADES) at the Oak Ridge National Laboratory, which is supported by the Office of Science of the U.S. Department of Energy under Contract No. DE-AC05-00OR22725. The contributions of M.D. Mihai, D. Iancu and G. Velişa to this work were also supported by a grant of the Romanian Ministry of Education and Research, CNCS—UEFISCDI, project number PN-III-P4- IDPCE2020- 1379, within PNCDI III. EZ (theory and simulation works) was supported by the Center for Nanophase Materials Sciences, (CNMS), which is a US Department of Energy, Office of Science User Facility at Oak Ridge National Laboratory. The contribution of W.J. Weber was supported by the National Science Foundation under Grant No. DMR-2104228. YZ is supported through the Laboratory Directed Research and Development Program at Idaho National Laboratory under the Department of Energy (DOE) Idaho Operations Office (an agency of the U.S. Government) Contract DE-AC07-05ID145142. Y.T. gratefully acknowledges the financial support by Taishan Scholars Program of Shandong Province (tsqn202103052), Yantai city matching fund for Taishan Scholars Program of Shandong Province.

References

[1] J.T. Yates, A New Opportunity in Silicon-Based Microelectronics, Science (1979). 279 (1998) 335–336. https://doi.org/10.1126/SCIENCE.279.5349.335.

[2] S.E. Thompson, S. Parthasarathy, Moore's law: the future of Si microelectronics, Materials Today. 9 (2006) 20–25. https://doi.org/10.1016/S1369-7021(06)71539-5.

[3] J.P. Dehollain, J.T. Muhonen, K.Y. Tan, A. Saraiva, D.N. Jamieson, A.S. Dzurak, A. Morello, Single-shot readout and relaxation of singlet and triplet states in exchange-coupled P 31 electron spins in silicon, Phys Rev Lett. 112 (2014) 236801. https://doi.org/10.1103/PHYSREVLETT.112.236801/FIGURES/4/MEDIUM.

[4] J.F. Gibbons, Ion implantation in semiconductors—Part II: Damage production and annealing, Proceedings of the IEEE. 60 (1972) 1062–1096. https://doi.org/10.1109/PROC.1972.8854.

[5] P.K. Sahoo, T. Som, D. Kanjilal, V.N. Kulkarni, Swift heavy ion beam induced recrystallization of amorphous Si layers, Nucl Instrum Methods Phys Res B. 240 (2005) 239–244. https://doi.org/10.1016/J.NIMB.2005.06.123.

[6] K. Cho, M. Numan, T.G. Finstad, W.K. Chu, J. Liu, J.J. Wortman, Transient enhanced diffusion during rapid thermal annealing of boron implanted silicon, Appl Phys Lett. 47 (1985) 1321–1323. https://doi.org/10.1063/1.96267.

[7] F.F. Morehead, R.F. Lever, Enhanced "tail" diffusion of phosphorus and boron in silicon: Self-interstitial phenomena, Appl Phys Lett. 48 (1986) 151–153. https://doi.org/10.1063/1.96980.

[8] S.C. Jain, W. Schoenmaker, R. Lindsay, P.A. Stolk, S. Decoutere, M. Willander, H.E. Maes, Transient enhanced diffusion of boron in Si, J Appl Phys. 91 (2002) 8919. https://doi.org/10.1063/1.1471941.

[9] G. Hobler, G. Otto, Status and open problems in modeling of as-implanted damage in silicon, Mater Sci Semicond Process. 6 (2003) 1–14. https://doi.org/10.1016/S1369-8001(03)00065-9.

[10] M. Toulemonde, J. Dural, G. Nouet, P. Mary, J.F. Hamet, M.F. Beaufort, J.C. Desoyer, C. Blanchard, J. Auleytner, High Energy Heavy Ion Irradiation of Silicon, Physica Status Solidi (a). 114 (1989) 467–473. https://doi.org/10.1002/PSSA.2211140205.

[11] P. Mary, P. Bogdanski, M. Toulemonde, R. Spohr, J. Vetter, Deep-level transient spectroscopy studies of U-irradiated silicon, Nucl Instrum Methods Phys Res B. 62 (1992) 391–393. https://doi.org/10.1016/0168-583X(92)95263-Q.

[12] W. Wesch, E. Wendler, Ion beam modification of solids : ion-solid interaction and radiation damage, 2016. https://doi.org/10.1007/978-3-31933561-2.

[13] Y. Zhang, W.J. Weber, Ion irradiation and modification: The role of coupled electronic and nuclear energy dissipation and subsequent nonequilibrium processes in materials, Appl Phys Rev. 7 (2020) 041307. https://doi.org/10.1063/5.0027462.

[14] L. Thomé, G. Gutierrez, I. Monnet, F. Garrido, A. Debelle, Ionization-induced annealing in silicon upon dual-beam irradiation, J Mater Sci. 55 (2020) 5938–5947. https://doi.org/10.1007/S10853-020-04399-8/FIGURES/7.

[15] L. Pelaz, L.A. Marqús, J. Barbolla, Ion-beam-induced amorphization and recrystallization in silicon, J Appl Phys. 96 (2004) 5947. https://doi.org/10.1063/1.1808484.

[16] J.B. Wallace, S. Charnvanichborikarn, L.B. Bayu Aji, M.T. Myers, L. Shao, S.O. Kucheyev, Radiation defect dynamics in Si at room temperature studied by pulsed ion beams, J Appl Phys. 118 (2015) 135709. https://doi.org/10.1063/1.4932209.

[17] J.B. Wallace, L.B.B. Aji, L. Shao, S.O. Kucheyev, Deterministic Role of Collision Cascade Density in Radiation Defect Dynamics in Si, Phys Rev Lett. 120 (2018) 216101. https://doi.org/10.1103/PHYSREVLETT.120.216101/FIGURES/4/MEDIUM.

[18] J.B. Wallace, L.B. Bayu Aji, L. Shao, S.O. Kucheyev, Impact of pre-existing disorder on radiation defect dynamics in Si, Scientific Reports 2019 9:1. 9 (2019) 1–7. https://doi.org/10.1038/s41598-019-48415-7.
[19] A. Dunlop, G. Jaskierowicz, S. Della-Negra, Latent track formation in silicon irradiated by 30 MeV fullerenes, Nucl Instrum Methods Phys Res B. 146 (1998) 302–308. https://doi.org/10.1016/S0168-583X(98)00509-6.
[20] B. Canut, N. Bonardi, S.M.M. Ramos, S. Della-Negra, Latent tracks formation in silicon single crystals irradiated with fullerenes in the electronic regime, Nucl Instrum Methods Phys Res B. 146 (1998) 296–301. https://doi.org/10.1016/S0168-583X(98)00512-6.
[21] H. Amekura, M. Toulemonde, K. Narumi, R. Li, A. Chiba, Y. Hirano, K. Yamada, S. Yamamoto, N. Ishikawa, N. Okubo, Y. Saitoh, Ion tracks in silicon formed by much lower energy deposition than the track formation threshold, Scientific Reports 2021 11:1. 11 (2021) 1–11. https://doi.org/10.1038/s41598-020-80360-8.
[22] D. Iancu, E. Zarkadoula, M.D. Mihai, C. Burducea, I. Burducea, M. Straticiuc, Y. Zhang, W.J. Weber, G. Velişa, Revealing two-stage phase transition process in defective KTaO3 under inelastic interactions, Scr Mater. 222 (2023) 115032. https://doi.org/10.1016/J.SCRIPTAMAT.2022.115032.
[23] L. Thomé, A. Debelle, F. Garrido, P. Trocellier, Y. Serruys, G. Velisa, S. Miro, Combined effects of nuclear and electronic energy losses in solids irradiated with a dual-ion beam, Appl Phys Lett. 102 (2013) 141906. https://doi.org/10.1063/1.4801518.
[24] A. Debelle, G. Gutierrez, A. Boulle, F. Garrido, O. Najjar, E. Olebunne, F. Pallier, C. Cabet, L. Thomé, Disordering kinetics in monocrystalline and epitaxial Si upon energy deposition induced by dual-beam ion irradiation, Appl Phys A Mater Sci Process. 127 (2021) 1–9. https://doi.org/10.1007/S00339-021-04890-2/FIGURES/6.
[25] K.T. Luketić, M. Karlušić, A. Gajović, S. Fazinić, J.H. O'Connell, B. Pielić, B. Radatović, M. Kralj, Investigation of Ion Irradiation Effects in Silicon and Graphite Produced by 23 MeV I Beam, Materials 2021, Vol. 14, Page 1904. 14 (2021) 1904. https://doi.org/10.3390/MA14081904.
[26] M.D. Mihai, P. Ionescu, D. Pantelica, H. Petrascu, D. Craciun, V. Craciun, F. Vasiliu, B.S. Vasile, I. Mercioniu, Annealing of preexisting defects in silicon single crystals by ion irradiation, Nucl Instrum Methods Phys Res B. 450 (2019) 85–89. https://doi.org/10.1016/J.NIMB.2018.09.005.
[27] J. Linnros, B. Svensson, G. Holmén, Ion-beam-induced epitaxial regrowth of amorphous layers in silicon on sapphire, Phys Rev B. 30 (1984) 3629. https://doi.org/10.1103/PhysRevB.30.3629.
[28] J.S. Williams, G. de, H. Bernas, F. Fortuna, Ion-beam-induced amorphization and epitaxial crystallization of Silicon, Topics in Applied Physics. 116 (2010) 73–111. https://doi.org/10.1007/978-3-540-88789-8_4.
[29] F. Priolo, E. Rimini, Ion-beam-induced epitaxial crystallization and amorphization in silicon, Materials Science Reports. 5 (1990) 321–379. https://doi.org/10.1016/0920-2307(90)90003-L.
[30] P.K. Sahoo, T. Mohanty, D. Kanjilal, A. Pradhan, V.N. Kulkarni, Epitaxial recrystallization of amorphous Si layers by swift heavy ions, Nucl Instrum Methods Phys Res B. 257 (2007) 244–248. https://doi.org/10.1016/J.NIMB.2007.01.008.
[31] S. Bhakta, I. Sulania, S. Ojha, D. Kanjilal, P.K. Sahoo, Swift heavy ion beam stimulated epitaxial recrystallization of Si/SiO2 heterostructure, Mater Lett. 308 (2022) 131153. https://doi.org/10.1016/J.MATLET.2021.131153.

[32] J.S. Williams, M.C. Ridgway, R.G. Elliman, J.A. Davies, S.T. Johnson, G.R. Palmer, MeV ion-beam annealing of semiconductor structures, Nucl Instrum Methods Phys Res B. 55 (1991) 602–606. https://doi.org/10.1016/0168-583X(91)96240-L.
[33] E. B∅gh, P. H∅gild, I. Stensgaard, Spatial distribution of defects in ion bombarded silicon and germanium, Radiat Eff. 7 (2006) 115–121. https://doi.org/10.1080/00337577108232571.
[34] W.H. Kool, H.E. Roosendaal, L.W. Wiggers, F.W. Saris, Production and beam annealing of damagein carbon implanted silicon. II, Radiat Eff. 36 (2006) 41–48. https://doi.org/10.1080/00337577808233169.
[35] T. Som, B. Satpati, O.P. Sinha, D. Kanjilal, Swift heavy-ion-induced epitaxial crystallization of buried Si3N4 layer, J Appl Phys. 98 (2005) 013532. https://doi.org/10.1063/1.1949275.
[36] O.W. Holland, Interaction of MeV ions with pre-existing damage in Si: A new ion beam annealing mechanism, Appl Phys Lett. 54 (1998) 320. https://doi.org/10.1063/1.100998.
[37] A. Kinomura, T. Yoshiie, A. Chayahara, Y. Mokuno, N. Tsubouchi, Y. Horino, Q. Xu, K. Sato, K. Yasuda, R. Ishigami, Neutron-enhanced annealing of ion-implantation induced damage in silicon heated by nuclear reactions, Nucl Instrum Methods Phys Res B. 334 (2014) 48–51. https://doi.org/10.1016/J.NIMB.2014.05.001.
[38] I. Burducea, M. Straticiuc, D.G. Ghiță, D.V. Moșu, C.I. Călinescu, N.C. Podaru, D.J.W. Mous, I. Ursu, N.V. Zamfir, A new ion beam facility based on a 3 MV Tandetron™ at IFIN-HH, Romania, Nucl Instrum Methods Phys Res B. 359 (2015) 12–19. https://doi.org/10.1016/J.NIMB.2015.07.011.
[39] G. Velişa, R.F. Andrei, I. Burducea, A. Enciu, D. Iancu, D.A. Mirea, A. Spiridon, M. Straticiuc, Joint research activities at the 3 MV Tandetron™ from IFIN-HH, The European Physical Journal Plus 2021 136:11. 136 (2021) 1–13. https://doi.org/10.1140/EPJP/S13360-021-02156-7.
[40] J.F. Ziegler, SRIM-2003, Nucl Instrum Methods Phys Res B. 219–220 (2004) 1027–1036. https://doi.org/10.1016/J.NIMB.2004.01.208.
[41] W.J. Weber, Y. Zhang, Predicting damage production in monoatomic and multi-elemental targets using stopping and range of ions in matter code: Challenges and recommendations, Curr Opin Solid State Mater Sci. 23 (2019) 100757. https://www.sciencedirect.com/science/article/pii/S1359028619300750?via%3Dihub (accessed July 22, 2019).
[42] E. Holmström, A. Kuronen, K. Nordlund, Threshold defect production in silicon determined by density functional theory molecular dynamics simulations, Phys Rev B Condens Matter Mater Phys. 78 (2008) 045202. https://doi.org/10.1103/PHYSREVB.78.045202/FIGURES/2/MEDIUM.
[43] I.T. Todorov, W. Smith, K. Trachenko, M.T. Dove, DL_POLY_3: New dimensions in molecular dynamics simulations via massive parallelism, J Mater Chem. 16 (2006) 1911–1918. https://doi.org/10.1039/b517931a.
[44] T. Kumagai, S. Izumi, S. Hara, S. Sakai, Development of bond-order potentials that can reproduce the elastic constants and melting point of silicon for classical molecular dynamics simulation, Comput Mater Sci. 39 (2007) 457–464. https://doi.org/10.1016/J.COMMATSCI.2006.07.013.
[45] E. Zarkadoula, R. Devanathan, W.J. Weber, M.A. Seaton, I.T. Todorov, K. Nordlund, M.T. Dove, K. Trachenko, High-energy radiation damage in zirconia: Modeling results, J Appl Phys. 115 (2014) 83507. https://doi.org/10.1063/1.4866989/373289.

[46] E. Zarkadoula, M. Toulemonde, W.J. Weber, Additive effects of electronic and nuclear energy losses in irradiation-induced amorphization of zircon, Appl Phys Lett. 107 (2015) 261902. https://doi.org/10.1063/1.4939110/235858.
[47] D.M. Duffy, A.M. Rutherford, Including the effects of electronic stopping and electron–ion interactions in radiation damage simulations, Journal of Physics: Condensed Matter. 19 (2006) 016207. https://doi.org/10.1088/0953-8984/19/1/016207.
[48] E. Zarkadoula, S.L. Daraszewicz, D.M. Duffy, M.A. Seaton, I.T. Todorov, K. Nordlund, M.T. Dove, K. Trachenko, Electronic effects in high-energy radiation damage in iron, Journal of Physics: Condensed Matter. 26 (2014) 085401. https://doi.org/10.1088/0953-8984/26/8/085401.
[49] E. Zarkadoula, G. Samolyuk, H. Xue, H. Bei, W.J. Weber, Effects of two-temperature model on cascade evolution in Ni and NiFe, Scr Mater. 124 (2016) 6–10. https://doi.org/10.1016/j.scriptamat.2016.06.028.
[50] S.L. Daraszewicz, D.M. Duffy, Extending the inelastic thermal spike model for semiconductors and insulators, Nucl Instrum Methods Phys Res B. 269 (2011) 1646–1649. https://doi.org/10.1016/J.NIMB.2010.11.031.
[51] G.S. Khara, S.T. Murphy, S.L. Daraszewicz, D.M. Duffy, The influence of the electronic specific heat on swift heavy ion irradiation simulations of silicon, Journal of Physics: Condensed Matter. 28 (2016) 395201. https://doi.org/10.1088/0953-8984/28/39/395201.
[52] A. Akkerman, M. Murat, Electron–phonon interactions in silicon: Mean free paths, related distributions and transport characteristics, Nucl Instrum Methods Phys Res B. 350 (2015) 49–54. https://doi.org/10.1016/J.NIMB.2015.03.024.
[53] C. Dufour, V. Khomenkov, G. Rizza, M. Toulemonde, Ion-matter interaction: the three-dimensional version of the thermal spike model. Application to nanoparticle irradiation with swift heavy ions, J Phys D Appl Phys. 45 (2012) 065302. https://doi.org/10.1088/0022-3727/45/6/065302.
[54] J.A. Davies, G. Foti, L.M. Howe, J.B. Mitchell, K.B. Winterbon, Polyatomic-Ion Implantation Damage in Silicon, Phys Rev Lett. 34 (1975) 1441. https://doi.org/10.1103/PhysRevLett.34.1441.
[55] L. Nuckols, M.L. Crespillo, C. Xu, E. Zarkadoula, Y. Zhang, W.J. Weber, Coupled effects of electronic and nuclear energy deposition on damage accumulation in ion-irradiated SiC, Acta Mater. 199 (2020) 96–106. https://doi.org/10.1016/J.ACTAMAT.2020.08.014.
[56] J.S. Williams, R.G. Elliman, W.L. Brown, T.E. Seidel, Dominant Influence of Beam-Induced Interface Rearrangement on Solid-Phase Epitaxial Crystallization of Amorphous Silicon, Phys Rev Lett. 55 (1985) 1482. https://doi.org/10.1103/PhysRevLett.55.1482.
[57] Y. Zhang, H. Xue, E. Zarkadoula, R. Sachan, C. Ostrouchov, P. Liu, X. Wang, S. Zhang, T.S. Wang, W.J. Weber, Coupled electronic and atomic effects on defect evolution in silicon carbide under ion irradiation, Curr Opin Solid State Mater Sci. 21 (2017) 285–298. https://doi.org/10.1016/J.COSSMS.2017.09.003.
[58] W.J. Weber, H. Xue, E. Zarkadoula, Y. Zhang, Two regimes of ionization-induced recovery in SrTiO3 under irradiation, Scr Mater. 173 (2019) 154–157. https://doi.org/10.1016/J.SCRIPTAMAT.2019.08.013.

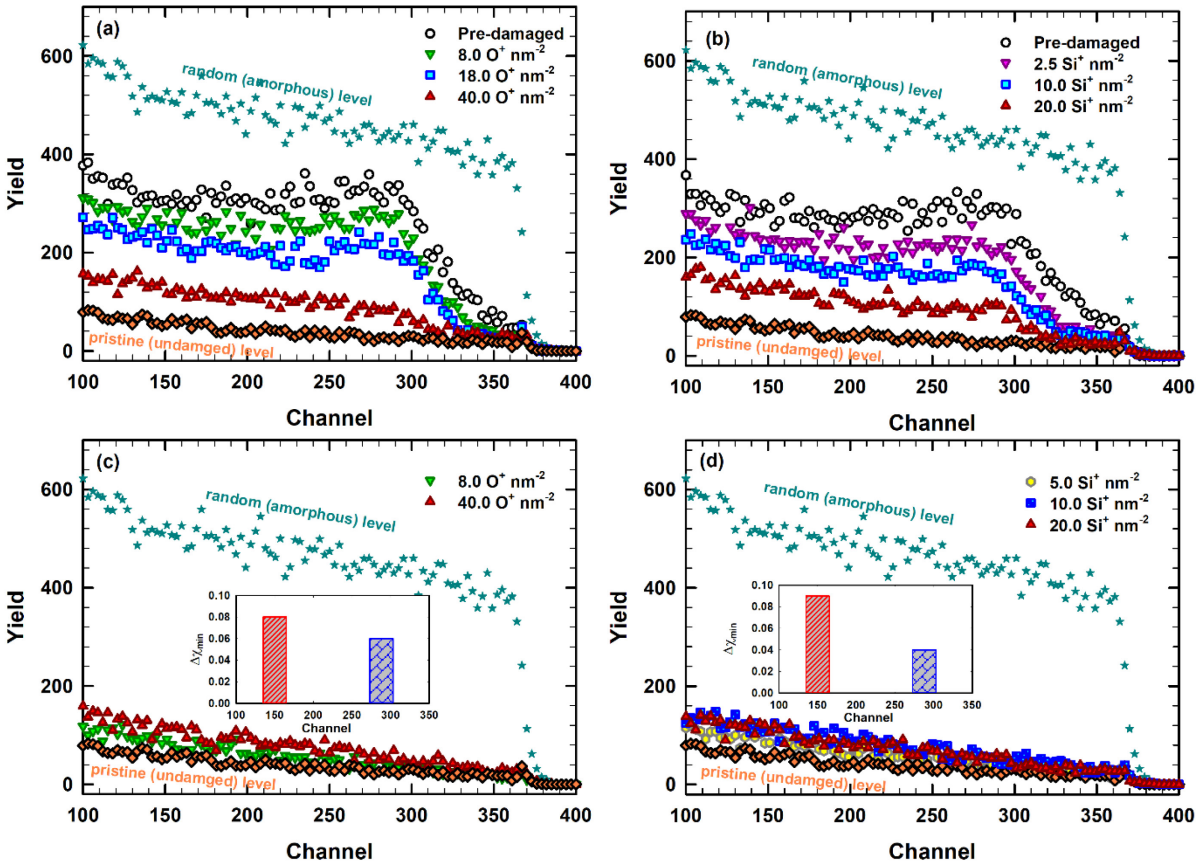

Fig. 1. The RBS/C spectra recorded for (a) pre-damaged and (c) pristine Si single crystals irradiated at 300 K with 12 MeV O ions at the indicated fluences. For comparison, RBS results for (b) pre-damaged and (d) pristine Si single crystals irradiated at 300 K with 12 MeV Si ions are also illustrated. Note the RBS spectra recorded in random and channeling direction from a pristine crystal are also shown. Inset: the difference in minimum yield of irradiated and pristine (unirradiated) crystalline sample as calculated for channel number 150 (i.e. deeper depth) and 288 (at Au-induced damage peak).

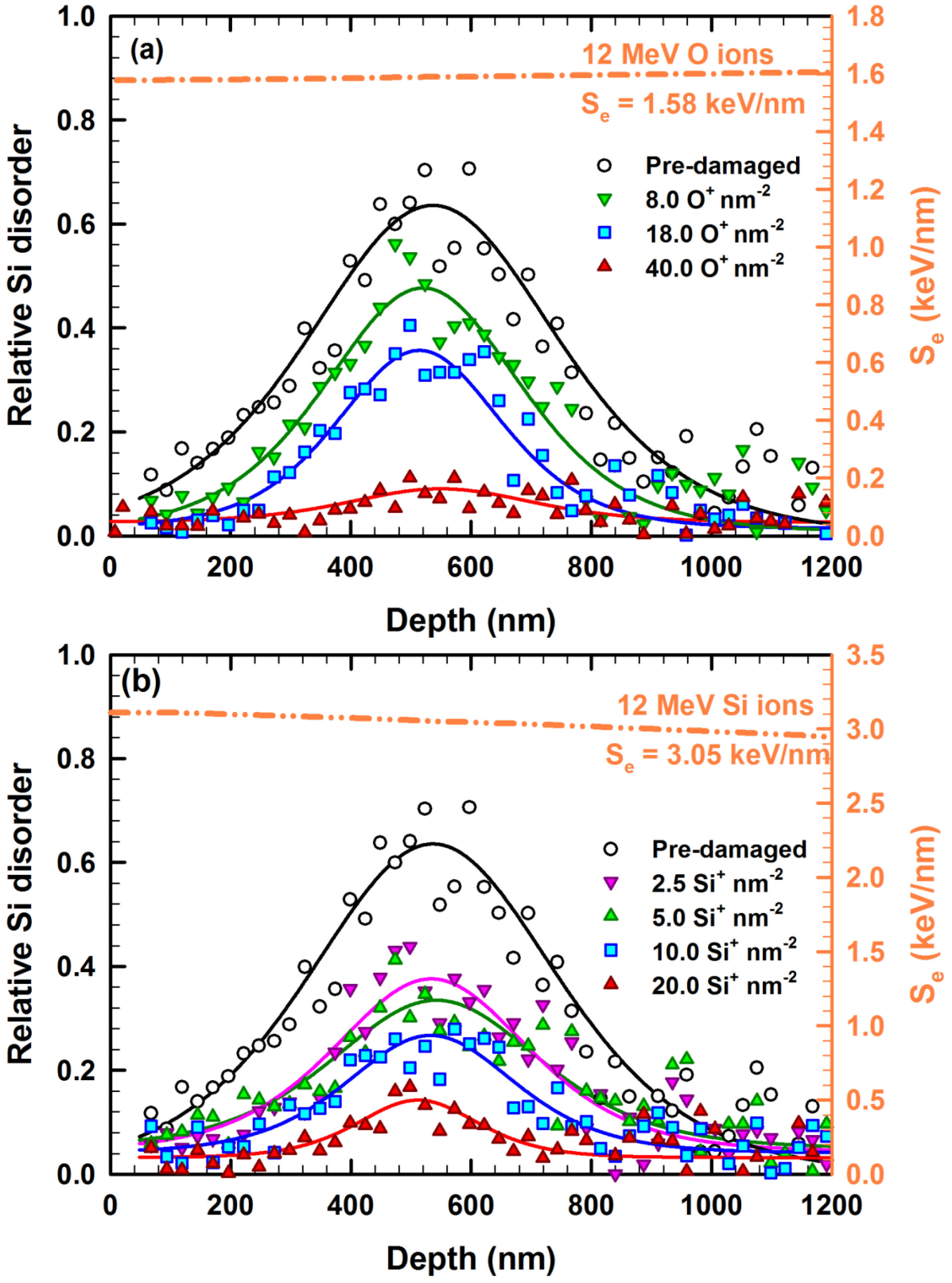

Fig. 2. Relative Si disorder profiles for pre-damaged Si single crystals with a maximum initial disorder fraction $f_0 \sim 0.7$ and sequentially irradiated with: (a) 12 MeV O ions and (b) 12 MeV Si ions at the indicated ion fluences. Also superimposed are the SRIM-derived S_e curves (orange dash-dot lines).

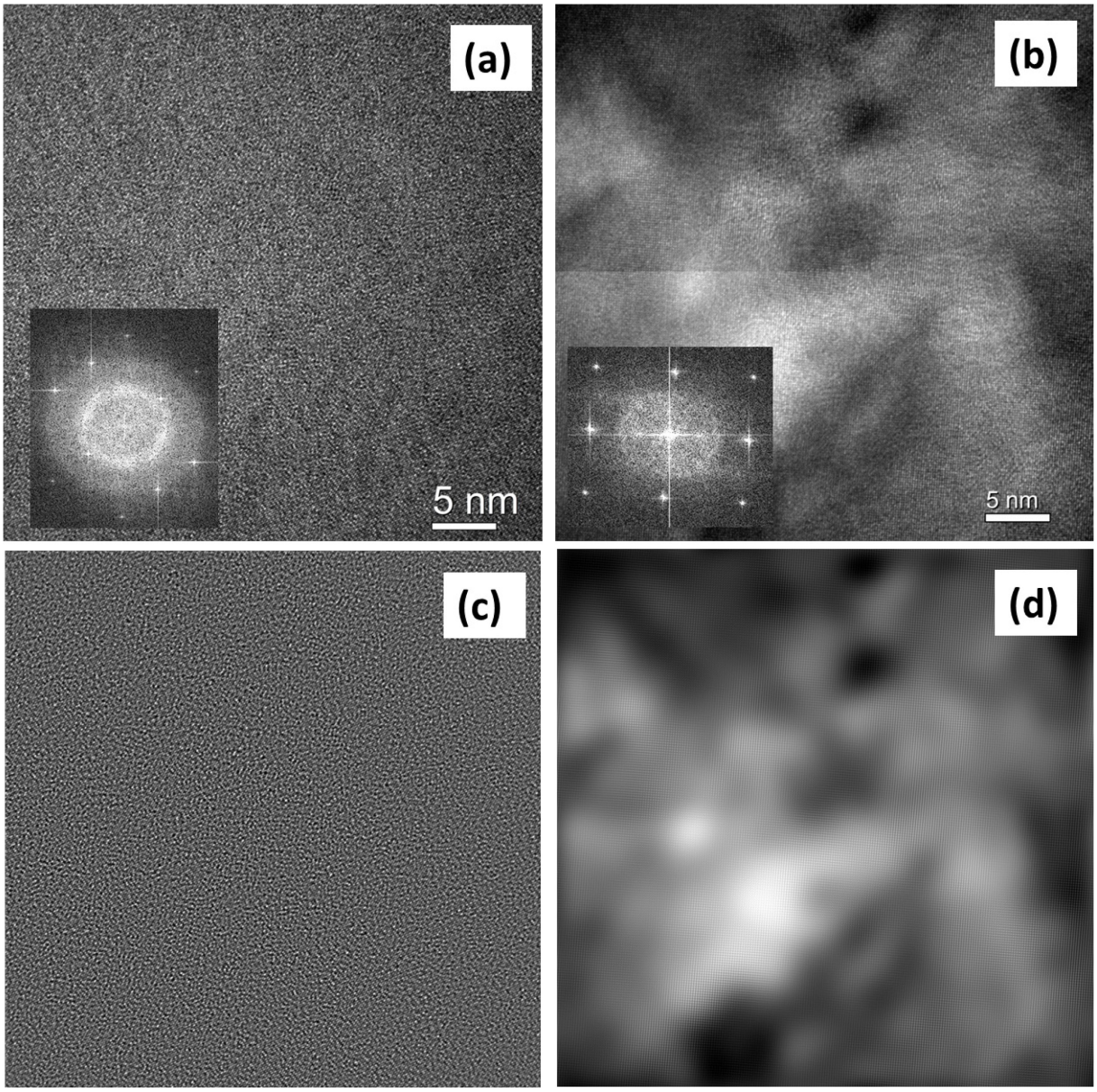

Fig. 3. HRTEM micrographs showing the microstructure changes of the Si single crystals: (a) pre-damaged with 2.0 MeV Au ions to ion fluence of 0.3 ions nm^{-2} at 300 K and (b) subsequently irradiated with 12 MeV O ions to ion fluence of 40.0 ions nm^{-2} at 300 K. The corresponding processed images are shown in (c) and (d), respectively. Note that the HRTEM micrographs were recorded at Au-induced damage peak (~532 nm).

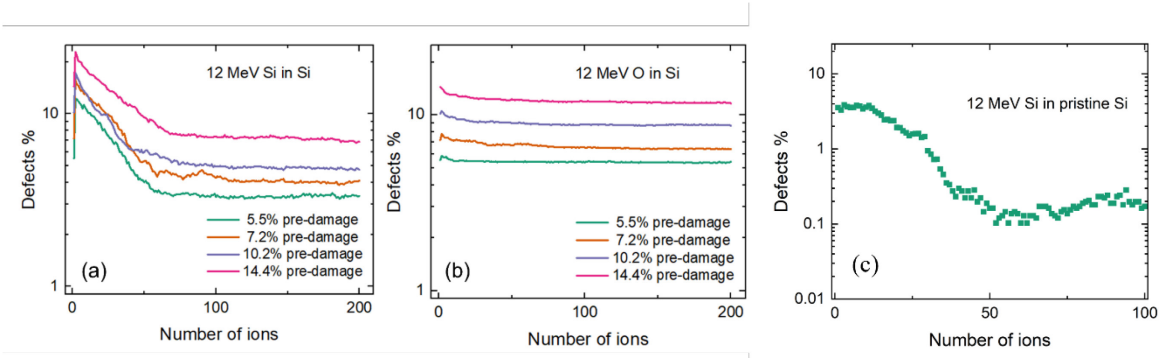

Fig. 4. Evolution of defect level in Si with increasing number of 12 MeV Si ions (a) and 12 MeV O ions (b) for four systems with different initial levels of pre-existing defects. For comparison, damage evolution in the pristine sample for increasing number of Si ions is also provided (Fig. 4(c)).

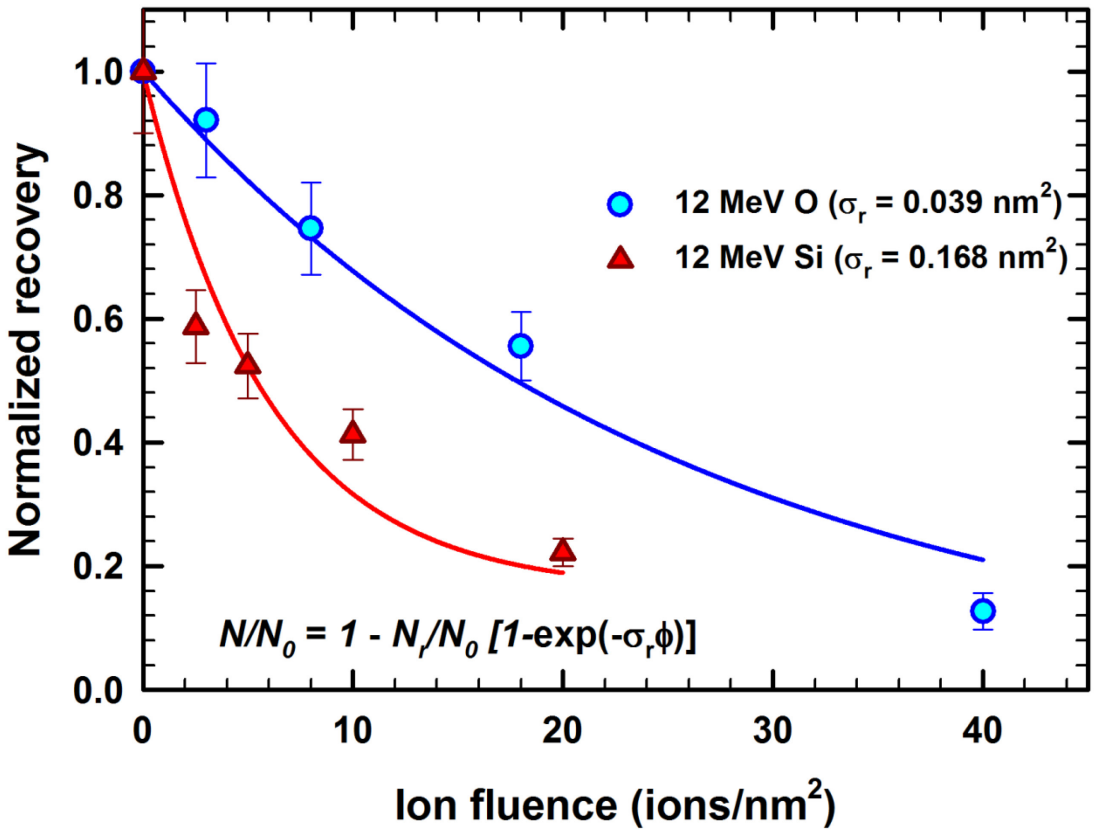

Fig. 5. Comparison of normalized recovery dependence on the ion fluence for O (filled circle) and Si (filled triangles) ion irradiations obtained from the analysis of RBS/C data. Solid curves are a fit of Eq. (1) to the experimental results.